Organic & Biomolecular Chemistry

Cite this: *Org. Biomol. Chem.*, 2012, **10**, 2798

www.rsc.org/obc

PAPER

Hybrid ligand–alkylating agents targeting telomeric G-quadruplex structures†

Filippo Doria,[a] Matteo Nadai,[b] Marco Folini,[c] Marco Di Antonio,[d] Luca Germani,[a] Claudia Percivalle,[a] Claudia Sissi,[d] Nadia Zaffaroni,[c] Stefano Alcaro,[e] Anna Artese,[e] Sara N. Richter*[b] and Mauro Freccero*[a]

Received 29th October 2011, Accepted 17th January 2012
DOI: 10.1039/c2ob06816h

The synthesis, physico-chemical properties and biological effects of a new class of naphthalene diimides (NDIs) capable of reversibly binding telomeric DNA and alkylate it through an electrophilic quinone methide moiety (QM), are reported. FRET and circular dichroism assays showed a marked stabilization and selectivity towards telomeric G4 DNA folded in a hybrid topology. NDI–QMs' alkylating properties revealed a good reactivity on single nucleosides and selectivity towards telomeric G4. A selected NDI was able to significantly impair the growth of melanoma cells by causing telomere dysfunction and down-regulation of telomerase expression. These findings points to our hybrid ligand–alkylating NDIs as possible tools for the development of novel targeted anticancer therapies.

Introduction

A hallmark of cancer cells is their limitless proliferative potential,[1] which is sustained by the activation of a telomere maintenance mechanism (TMM), namely telomerase and the alternative lengthening of telomere (ALT) mechanisms.[2] Telomeres are specialized DNA–protein structures located at the end of eukaryotic chromosomes and serve to protect them from degradation, recombination and inappropriate DNA repair events.[3] Human telomeric DNA consists of tandem repeats of the T_2AG_3 sequence terminating with a 3′ single-stranded overhang (telomeric 3′-overhang).[3]

Telomere maintenance is essential for the transformation of most human cancer cells, and the activation of a TMM is crucial to escape a crisis and allow cells to become immortalized. In a high percentage of human tumors (>85%), telomeres are maintained by telomerase reactivation,[2] whereas in about 15% of tumors lacking telomerase (frequently of mesenchymal and neuroepithelial origin)[4] telomeres are maintained by ALT mechanisms.[5] Data obtained from preclinical studies concerning the effects of telomerase inhibition have provided compelling arguments to indicate that the enzyme is a well-validated cancer target.[6] However, telomerase-based cancer therapeutics is moving very slowly to the clinical setting. The only telomerase inhibitor currently being tested in clinical trials is the template antagonist imetelstat.[7] In addition, lack of knowledge about the molecular determinants of ALT mechanisms makes it difficult to design and develop therapies to selectively interfere with telomere homeostasis in tumors that do not express telomerase.

Under physiological conditions, G-rich sequences are capable of generating a four-stranded helical structure, known as G-quadruplex (G4), which forms when four units of guanine are present in a square planar arrangement.[8] G4s exhibit extensive structural polymorphism and may form intramolecular or intermolecular DNA strands.[8] The elucidation of the crystal and solution structures of telomeric G4 has led to the rational development of effective G4-stabilizing small molecules.[2] Common features shared by G4 ligands are the potential for a flat conformation and the presence of cationic or protonable moieties.[9] This characteristic can be modulated in order to improve the specific recognition of quadruplex-over duplex-DNA and between different (by sequence and topology) G4 structures. An improvement in G4 targeting has recently been obtained by tethering electrophilic Pt(II) complexes to a quinacridine unit as G4 ligand. Such a strategy allows a "dual covalent–noncovalent binding mode" to

[a]*Dipartimento di Chimica, Università di Pavia, V.le Taramelli 10, 27100 Pavia, Italy. E-mail: mauro.freccero@unipv.it; Fax: +39 0382987323; Tel: +39 038298668*
[b]*Dipartimento di Medicina Molecolare, Via Gabelli 63, 35121 Padova, Italy. E-mail: sara.richter@unipd.it*
[c]*Dipartimento di Oncologia Sperimentale e Medicina Molecolare, Fondazione IRCCS Istituto Nazionale dei Tumori, Via G. Amadeo 42, 20133 Milano, Italy*
[d]*Department of Pharmaceutical and Pharmacological Sciences, Università di Padova, Via Marzolo 5, 35131 Padova, Italy*
[e]*Dipartimento di Scienze della Salute, Università degli Studi "Magna Græcia" di Catanzaro, Campus Universitario "S. Venuta", 88100 Catanzaro, Italy*

†Electronic supplementary information (ESI) available: Details about experimental procedures concerning the synthesis and structural characterization of the intermediates **8–14**, and the NDIs **1**, **1Br**, **3**, **3Br**, **4**, **5Br**, **6**, DNA alkylation, telomerase activity assay and western immunoblotting are provided in Supplementary Experimental Procedures. FRET-melting and CD analysis were performed as recently reported (ref. 14). See DOI: 10.1039/c2ob06816h

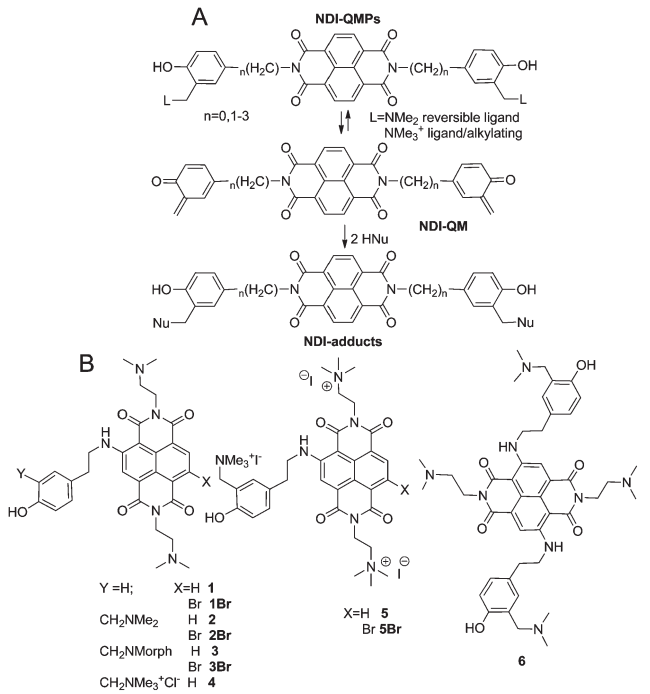

Scheme 1 (A) Naphthalene diimmides conjugated to quinone methide precursors (**NDI–QMPs**) recently investigated. (B) Substituted **NDIs** synthesized and tested as (i) G4 reversible ligands (**1–3**, **1Br–3Br**, and **6**) and (ii) hybrid ligand–alkylating agents (**4**, **5** and **5Br**).

be achieved by G4 platination, which should ensure a greater stabilization of the target.[9,10]

To avoid the problems related to the intrinsic reactivity of Pt(II) electrophiles, we recently developed the prototype of a new ligand where the naphthalendiimide core (**NDI**) was tethered to precursors (**NDI–QMPs**) of a reactive species such as quinone methides (**NDI–QM** in Scheme 1A).[11] In order to overcome poor water solubility of the resulting alkylated oligomers and to investigate separately the G4 reversible recognition and the subsequent alkylation, we have synthesized a new class of tri- and tetra-substituted NDIs (Scheme 1B) and investigated their reactivity and biochemical behavior towards G4 folded oligonucleotides. In addition, their potential as G4 ligands and selective telomere targeting agents has been investigated in *in vitro* established cancer cell lines.

Results and discussion

Rational design and synthesis of new NDI derivatives

The addition of alkyl-amino side chains to di-substituted NDIs, giving tri- and tetra-substituted NDIs improved dramatically the G4 binding properties,[12] and enhanced the selectivity for the parallel topology.[13] This evidence prompted us to translate this structural feature also to the alkylating NDIs already developed by our group (Scheme 1A), in order to improve the interactions with telomeric DNA.[11,14] The new NDIs acting as G4 reversible ligands **1–2**, **1Br-2Br** and **6** together with the potential ligand–alkylating hybrid structures **3–5**, **3Br** and **5Br** (Scheme 1B), differ from the previously synthesized **NDI–QMPs**[11] for the

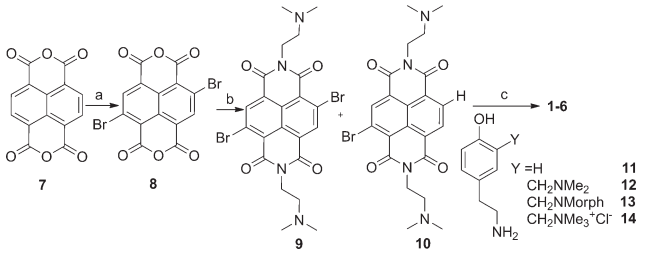

Scheme 2 Reagents and conditions: (a) dibromoisocyanuric acid (DBI), H_2SO_4, reflux, 12 h, yield 93% of **8**; (b) dimethylethylamine, glacial acetic acid, 130 °C, 30 min; (c) nucleophilic aromatic substitution S_NAr.

Table 1 Reactants and conditions for the key S_NAr (step c) on the dibrominated NDI **9**

Reactant	Conditions[a]	Products (%, yield)
11	MW, 3 min	**1** (66), **1Br** (37)
11	r.t., 8 h	**1** (15), **1Br** (74)
12	MW, 3 min	**2** (35), **2Br** (62)
12	MW, 5 min	**2** (25), **2Br** (40), **6** (30)
12	MW, 10 min	**2** (5), **6** (70)
13	r.t., 24 h	**3** (12), **3Br** (45)
14	r.t., 48 h	**4** (6)

NDI derivatives selectively bind human telomeric G4 folded DNA. [a] Reaction performed in DMF, under argon, at r.t. or microwaved assisted (MW, 180 °C, 250 psi, 200 W).

tethering position of the QMP, directly anchored to the aromatic ring, and for the presence of two unreactive and conformational flexible cationic moieties under physiological conditions. These modifications led to new molecules that retain the alkylation efficiency (**3–5**, **3Br** and **5Br**), as well as strongly improve the selectivity and the binding affinity towards the target. The new NDIs were expected to behave as (i) G4 reversible ligands (**1**, **2**, **1Br**, **2Br** and **6**) and (ii) hybrid ligand–alkylating agents (**3–5**, **3Br** and **5Br**, Scheme 1B) according to the nature of the leaving group at the benzyl position. The tri- and tetra-substituted NDIs exhibit two cationic side chains on the imides moieties [$(CH_2)_2NHMe_2^+$, or $(CH_2)_2NMe_3^+$] and a Mannich base, or its quaternary ammonium salt, directly tethered to the NDI aromatic core by a 2-aminoethyl spacer. Such a variety of the side chains used has been selected to evaluate the G4 binding properties and to switch on–off the alkylating properties of the resulting NDIs under mild thermal digestions (T = 40 °C). To synthesize the above tri- and tetra-substituted NDIs, we defined a new and efficient three-step synthetic route (Scheme 2) to tether the cationic arms and the reactive moiety to the imide group and to the NDI core, respectively.

Briefly, the synthesis requires two key orthogonal steps, an imidization (step b, Scheme 2) and a nucleophilic aromatic substitution (S_NAr, step c) using the *ortho* functionalized tyramine derivatives (**11–14**). The S_NAr affording the G4 reversible ligands **1**, **2**, **1Br**, **2Br** and **6** have been performed following a microwave-assisted (MW) protocol (Table 1). Unfortunately, this was unsuitable for the synthesis of the potential hybrid ligand–alkylating agents **3–5**, **3Br** and **5Br**, bearing a thermally reactive

Table 2 $\Delta T_{1/2}$ of reversible binding at 0.8 μM NDI, measured by FRET of the labeled oligomer F21T[a] in K^+ solution

NDI	$\Delta T_{1/2}$/°C (0.8 μM)
2	22.2 ± 0.3
2Br	20.3 ± 0.8
1	18.2 ± 0.3
1Br	15.6 ± 0.5
3	4.5 ± 0.4
6	3.2 ± 0.6

[a] d(*FAM*-$G_3[T_2AG_3]_3$-*Tamra*); *FAM*: 6-carboxyfluorescein and *Tamra*: 6-carboxy-tetramethylrhodamine.

QMP moiety. In fact, under the harsh conditions required by the S_NAr, the QMP moieties of the NDIs **3**, **3Br** and **4** underwent fast degradation through QM generation. To avoid such a limit, we have optimized an original protocol for the mono-functionalization *via* S_NAr reaction at r.t. (Table 1).

NDI derivatives selectively bind human telomeric G4 folded DNA

FRET-melting experiments were initially carried out to evaluate the stabilization and selectivity of reversible-binding NDIs **1–3**, **1Br–3Br** and **6** for F21T, an oligomer bearing the human telomeric DNA sequence. The FRET-melting data (Table 2) demonstrated that derivatives **2** and **2Br** effectively stabilize the telomeric G4, with $\Delta T_{1/2}$ values above 20 °C. Derivative **2** had the most important effect on telomeric G4 stabilization, with a $\Delta T_{1/2}$ value of 22.2 °C, which is slightly lower than $\Delta T_{1/2}$ values ($6.2 < T_{1/2} < 28.2$ °C) of reported tri-substituted NDIs.[12] Compounds **1** and **1Br** were slightly less efficient ($\Delta T_{1/2}$ in the range of 15.6–18.2 °C), while the tetra-substituted NDI **6** and the morpholine derivative **3** were very poor stabilizers ($\Delta T_{1/2}$ = 3.2 °C and 4.5 °C, respectively).

These data are in striking contrast to the excellent binding properties of other tetra-substituted NDIs[12] and suggest that the NDI can accommodate only one aromatic bulky moiety tethered to the NDI core without losing the promising G4 binding properties. Compounds **4**, **5** and **5Br** were not included, because high temperature would have activated them triggering alkylation.

The selectivity towards G4 was assessed for all compounds by a FRET-based competition assay, by which the ability of ligands to retain G4 stabilizing affinity was challenged by non-fluorescent DNAs: a telomere non-related G4 forming DNA (27NHEG, cited as G4 in Fig. 1), duplex (ds26), or single-stranded scrambled G4 oligomers (ss), see Fig. 1.

The 27NHEG was the only DNA capable of effectively competing with the labeled sequence. In fact, at 27NHEG : F21T molar ratio of 1.5 about 50% decrease in $\Delta T_{1/2}$ was obtained, whereas at molar ratio of 5, a 100% decrease in $\Delta T_{1/2}$ was observed for all compounds. In the presence of various amounts of the competitor ds26, the thermal stabilization of F21T enhanced by the NDI compounds was affected only starting from ds26 : F21T molar ratio of 15, at which the decrease in the $\Delta T_{1/2}$ value was around 20% for all compounds (Fig. 1B and S1†). Conversely, scrambled G4 oligomer did not affect $\Delta T_{1/2}$

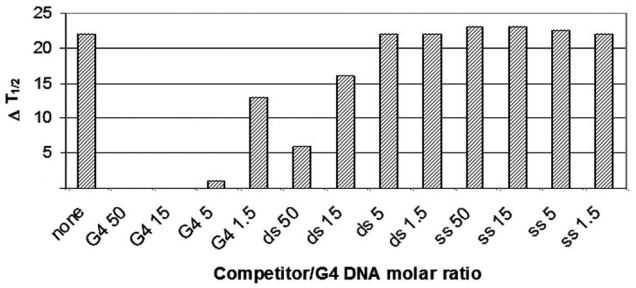

Fig. 1 FRET-based competition assay. Binding of NDI **2** to the fluorescence-labelled F21T oligo was challenged by a telomere non-related G4 forming DNA {27NHEG, for simplicity cited as G4: d(TGGGGAGGGTGGGGAGGGTGGGGAAGG)}, non-fluorescent duplex ds26 {ds: d(CAATCGGATCGAATTCGATCCGATTG)}, or single-stranded scrambled G4 DNA {ss: d(GGATGTGAGTGT-GAGTGTGAGG)}, each at 1.5, 5, 15, 50 competitor DNA:F21T molar ratio, in buffer containing 10 mM lithium cacodylate pH 7.4 and 50 mM KCl.

for any compound, at any molar ratio. These results demonstrated that our NDIs can be considered as a class of selective G4 ligands.

Modeling analysis

A molecular modeling analysis was used to better rationalize the different stabilizing effect of the NDI derivatives onto the telomeric G4. In particular the pharmacophoric properties of the ligands were investigated by the FLAP (Fingerprints for Ligands and Proteins) computational approach.[15,16] For all NDI analog the existence probability (p) of diverse tautomeric and protomeric forms was evaluated at pH 7.4 (Fig. S2A†). All possible forms showing $p > 1\%$ were submitted to a conformational analysis and all generated conformers were used to define a preliminary pharmacophoric model, characterized by the ligand molecular shape and by the hydrophobic, hydrogen bond donor and hydrogen bond acceptor molecular interaction fields (MIFs). In Fig. 2 the MIFs alignment is shown for all the studied NDIs, highlighting the superimposition of the ligands based on their interacting ability based on π–π stacking.

Thus the BASASA (Boltzmann Averaged Solvent Accessible Surface Area) method[17] was adopted in order to estimate the NDI scaffold accessibility, showing a wide accessible surface of **1** and **1Br** for DNA interactions (Fig. S2B†). However, their reduced stabilizing effect with respect to **2** and **2Br** could be attributed to a higher conformational flexibility, due to the loss of the Y substituent onto the 2-aminoethyl spacer, associated to an unfavorable entropic term. Moreover, the halogen was responsible for the electronic distribution and the steric hindrance of the NDI core, thus reducing the imide O potentiality to establish hydrogen bonds with the target. Conversely, **2** and **2Br**, associated to a wider accessible surface, exhibited a decreased conformational flexibility, thus allowing the protonated methyleneamino moiety to interact with the imide group and the phenolethylene side chain to come closer toward the NDI aromatic core. Although the accessible surface of NDIs **3** and **6** (Fig. 2) was not so different from that of the previous analogs, they exhibited a reduced core exposition able to interact with the

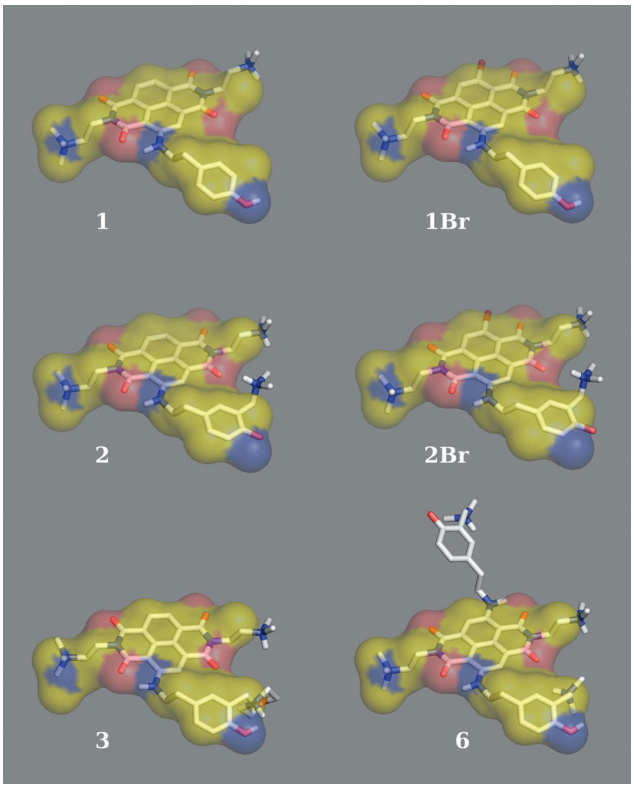

Fig. 2 Alignment of **1**, **1Br**, **2**, **2Br**, **3** and **6** NDIs (shown as polytube) with respect to the pharmacophoric model (represented as a transparent surface). The yellow, blue and red areas of the pharmacophoric surface indicate, respectively, the hydrophobic, the hydrogen bond donor and the hydrogen bond acceptor moieties.

target. Such an observation could be rationalized considering the intramolecular electrostatic interactions occurring between the morpholine and the ethyl-dimethylamino moieties of **3**. Specifically, the morpholine tertiary amino group, protonated at pH 7.4, was strongly attracted by the imide carbonyl; similarly the ethyl-dimethylamino side chain interacted with the morpholine oxygen. These contacts stabilized **3** in a conformation able to place the morpholine side chain perpendicularly with respect to the NDI aromatic core, thus hampering the interactions with the DNA. Finally, in the case of **6**, the presence of two phenol-ethylene side chains increased its conformational flexibility with a consequent unfavorable binding profile. In particular, the entropic term resulted disadvantaged, as well as the NDI core appeared bulkier and so less accessible to DNA.

CD analysis

It has been reported that the human telomeric DNA in K^+ solution folds in a 3 : 1 topology, in which three strands are oriented in one direction and the fourth is in the opposite direction, one loop is double-chain reversal and two are edgewise, one G-tetrad has *anti–syn–syn–syn* glycosidic conformation and two have a *syn–anti–anti–anti* conformation.[18] In circular dichroism (CD), this hybrid-type G4 conformation (mixed antiparallel–parallel topology) has shown a strong positive peak at 290 nm with a shoulder peak around 270 nm, and a smaller negative peak at

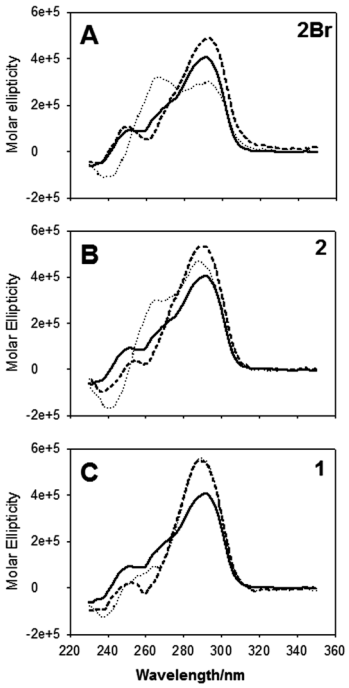

Fig. 3 CD analysis. Compounds **2Br** (A), **2** (B) and **1** (C) (16 μM) were incubated with hTel oligonucleotide (4 μM) after (dashed lines) or before (dotted lines) DNA annealing in the presence of K^+ 50 mM. The spectrum of hTel DNA annealed in the absence of NDIs is shown as a solid line.

235 nm.[18] In general, a positive band at 260 nm and a negative peak at 240 nm are characteristic of a parallel G4 topology,[13,19] while two positive bands at 290 nm and 245 nm, and a negative peak at 260 nm indicate an antiparallel G4 conformation.[20] To check the preferred G4 conformation stabilized by our NDIs, CD analysis of hTel DNA $\{d(AGGG[T_2AG_3]_3)\}$ upon binding with NDIs was performed. Compounds were added either before (~80 °C) or after folding (20 °C) of the G4 DNA. Clearly, annealing in the presence of the drug allows reaching a thermodynamically stable complex, whereas incubation in the absence of annealing will yield the fastest forming species.[21] Samples were left to equilibrate for 24 h before measurement of CD spectra. In these conditions hTel oligomer is present mainly as mixed–hybrid type topology as attested by a major positive peak at 290 nm and a shoulder at 270 nm (Fig. 3). Compounds **2**, **2Br**, and **1**, incubated after DNA folding, induced a comparable stabilization of the mixed–hybrid structure as proved by a similar increase in the positive peak at 290 nm (Fig. 3). However, when compounds were incubated before DNA folding, they showed a different behavior. In particular, upon **2** and **2Br** binding, the peak at 260 nm increased, the peak at 290 nm decreased and a minor negative peak at 240 nm appeared (Fig. 3A and B). This behavior could indicate a tendency to induce a parallel-like G4 topology, or alternatively may results from NDI interaction with the original conformation of the G4 DNA. This behavior is clear for **2Br**, and to a lesser extent for **2**, whereas **1** (and also **1Br**) did not show any significant difference (Fig. 3C), displaying a stabilization of the initial mixed–hybrid type topology under both incubation conditions.

Finally, the tetra-substituted NDI **6** behaved similarly to **1**, even if with a significantly reduced intensity. It has been reported that K^+ and Na^+ drive towards different conformations of the human telomeric sequence in solution.[13,19,20]

In particular, K^+ favors a mixed–hybrid type topology, while Na^+ stabilizes a full antiparallel conformation. We hence performed FRET-melting experiments in the presence of Na^+, instead of K^+, for compound **2**, the best performing NDI. Specifically, we found a $\Delta T_{1/2}$ value of 5.5 °C which, compared to 22.2 °C $\Delta T_{1/2}$ in K^+ in the same conditions, suggested a disfavored binding to a full antiparallel G4 conformation.

CD thermal unfolding experiments in the presence of **2** showed two different transitions: one at 290 nm (ΔT_m of 9.2 °C) and the other at 265 nm (ΔT_m of 18.8 °C) indicating a higher stabilization of the parallel-like conformation by the NDI (Fig. S3A and B†). The apparent ΔH value between the unfolding of the G4 DNA alone or in the presence of **2** was ~20 kcal mol^{-1}, indicating a strong stabilization of the G4 conformation upon drug binding. CD titrations with increasing drug : DNA molar ratios were used to assess stoichiometry of **2** against hTel DNA. Up to 4 molecules of drug were able to bind to one quadruplex molecule. This interaction was cooperative as shown by the slope of the Hill plot obtained from the CD titration data at two wavelengths. The results are consistent with an apparent Log K_d value of 23.95 and a cooperativity index of 4.01 using the Hill equation,[22] which confirms the presence of 4 interacting sites (Fig. S3 C–E†). Tetra-substituted NDI derivatives have been co-crystallized in a 6 : 2 stoichiometry with the parallel G4 conformation of the human telomeric DNA,[23] and have been shown to induce formation of a parallel G-quadruplex topology in solution.[13] Recently, only isaindigotone derivatives have been reported to bind in a 4 : 1 mode in solution, stabilizing the antiparallel topology of the human telomeric DNA.[24] Hence, our NDI compounds represent the first example of a 4 : 1 binding mode towards a parallel-like telomeric G4 conformation.

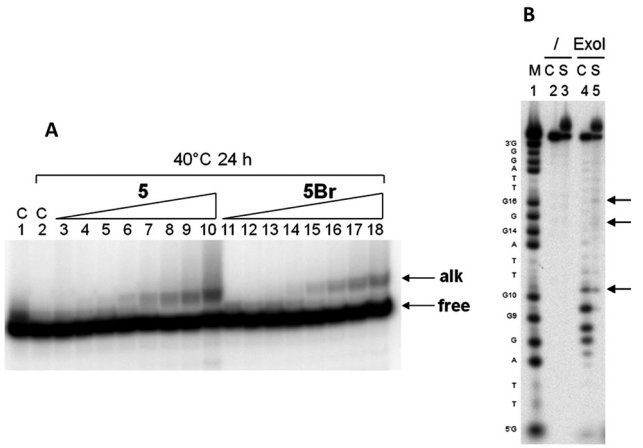

Fig. 4 hTel DNA alkylation and site analysis. (A) The ^{32}P-hTel oligo was incubated with increasing amounts of NDIs **5** and **5Br** (0.003–50 μM) at 40 °C to activate alkylation. The alkylated DNA (alk) was separated from the non-reacted DNA (free) by 20% polyacrylamide–7 M urea denaturing gel. (B) ExoI digestion of the adduct of compound **5** with hTel DNA. The adduct was gel-purified, digested with ExoI, run on a 20% denaturing polyacrylamide gel and visualized by phosphorimaging. The non-alkylated DNA was gel-purified and treated in the same condition as a control. M, C and S stand for Marker, Control and Sample. Arrows indicate the major slow-down sites (putative alkylation sites) in the purified adduct.

NDI–QMPs alkylate dC, dG, dA and G4 telomeric DNA

Since we have proven that NDIs can effectively and selectively recognize a G4-folded telomeric sequence, we also tested the ability of NDI–QMPs to covalently bind to G4 DNA. We first explored the alkylation properties of **5** against single nucleosides in solution. As gauged by HPLC, upon a 24 h incubation at 60 °C, **5** displayed reactivity towards deoxyguanosine (dG), 2′-deoxycytidine (dC) and 2′-deoxyadenosine (dA), even if with poor yields (9%, 12% and 1%, respectively). 2′-Deoxythymidine (dT) was not alkylated by **5**. Adduct characterization was performed for the most abundant, NDI:dG and NDI:dC (Fig. S4 A–C†). Mass spectrometry analysis showed that the reaction with dG formed an adduct corresponding to a positively double-charged molecule made by **5** and dG, with loss of ribose. Since the loss of ribose typically derives from alkylation at N7 of dG, we hypothesize that the attack of QM to dG-N7 is then followed by the loss of the sugar moiety. A second adduct corresponding to the attack of QM of another nucleophilic function of dG was found. Taking into account that the activations of NDI–QMPs have been performed under thermodynamic control and that the dG-N2 conjugate adduct with the prototype *o*-QM is the most stable alkylated product,[25,26] we can assume dG-N2 as the second alkylation site at the nucleoside structure. Regarding dC, one major adduct formed by the attack of the QM to a dC nucleophilic moiety. It has been reported that, under thermodynamic control, QM should react preferentially at the exocyclic NH_2 of dC, dG and dA.[27,28] Similar results were obtained for compounds **5Br** and **4** (data not shown).

We next investigated the alkylating ability of compounds **4**, **5**, and **5Br** on G4-folded telomeric sequence. The compounds induced the formation of an alkylation band that migrates slower than the non-alkylated hTel oligonucleotide (Fig. 4A). This behavior is a common feature of G4 alkylation with QM.[11,14] At the highest concentration (50 μM) the percentage of alkylated adducts was 12%, 7% and 5% for **5**, **5Br** and **4**, respectively (Fig. 4A and data not shown). Although the yield was modest, the formation of alkylated adducts was already appreciable at 12 nM **5** and 50 nM **5Br** (lanes 6 and 15, in Fig. 4A). In addition, the alkylation reaction was selective for G4-folded DNA. In fact, no discrete adducts were observed when **5** was incubated with a double-stranded nucleic acid (Fig. S4D†).

To detect the site of alkylation, the adduct band was gel-purified and subjected to digestion with Exonuclease I (ExoI), which catalyzes the removal of nucleotides from single-stranded-DNA in the 3′ to 5′ direction. As shown in Fig. 4B, the purified adduct was slightly unstable: in fact, around 30% of non-alkylated oligonucleotide re-formed. However, this behavior is not unexpected for alkylation adducts generated from electron rich QMs and has been already observed.[14] Only the covalent adducts at the exocyclic NH_2 groups of C, G and A moieties are thermodynamically stable, and alkylation adducts at different sites should revert to free QM and DNA. ExoI cut the control

Table 3 IC_{50} (μM) obtained in colon (HT29), lung (A549) and melanoma (SKMel-5) tumor cells after a 24 h exposure to different NDIs

NDIs	HT29	A549	SKMel-5
2	1.0 ± 0.1	1.2 ± 0.2	2.4 ± 0.1
2Br	1.0 ± 0.1	1.3 ± 0.1	n.a.[a]
1	1.25 ± 0.4	1.1 ± 0.1	1.9 ± 0.1
1Br	4.0 ± 1.4	3.2 ± 0.2	5.1 ± 0.5
3	1.2 ± 0.8	3.0 ± 1.1	2.8 ± 0.1
3Br	4.0 ± 1.3	9.0 ± 0.9	n.a.[a]
6	2.5 ± 0.7	7.6 ± 1.0	3.9 ± 0.4
4	0.4 ± 0.1	0.9 ± 0.1	n.a.[a]
5	>100	>100	>100
5Br	>100	>100	>100

[a] n.a.: not available.

non-alkylated hTel all throughout the sequence and presented a major slow-down region at G9 (numbering starting from the 5′-end, Fig. 4B). In contrast, the purified alkylation sample presented three major slow-down regions at the level of the second and third G repeats (G10 and G14–G16, indicated by arrows in Fig. 4B), which can be accounted for by the NDI putative alkylation sites. When the **5**-hTel adduct was incubated with hot piperidine, we failed to reveal any bond breakage (Fig. S4E†), suggesting that the alkylation of a G4-folded DNA does not involve the dG-N7. Therefore other available nucleophilic moieties must be involved in NDI alkylation. Unfortunately adduct instability prevented further characterization analysis.

Cytotoxic activity of NDIs

Short-term cytotoxic activity of NDIs was tested in three telomerase-positive human cancer cell lines. Data showed that, in at least two out of three cell models, the reversible ligands **2**, **2Br** and **1** were active at the low μM range, followed by compounds **3**, **1Br**, **6** and **3Br** (Table 3). Regarding the alkylating NDIs, **4** was the best performing compound, in terms of cytotoxicity, whereas the di-cationic **5** and **5Br** did not affect the growth of all three cell lines, likely as a consequence of their poor cellular uptake.

Compound 2 impairs the growth of human melanoma cells, induces telomere dysfunction and inhibits telomerase activity

The biological effects of **2**, the best G4 reversible binder (Table 2), were subsequently assessed in human melanoma SKMel-5 cells. Specifically, a 48 h exposure to increasing concentrations (from 0.05 to 50 μM) of **2**, resulted in a marked and dose-dependent inhibition of cell growth (Fig. 5A), with an IC_{50} of 1.7 ± 0.5 μM. It has been reported that G4-ligand-mediated impairment of cancer cell growth may occur as a consequence of drug-induced perturbations of telomere architecture.[2]

In this context, a 48 h exposure of SKMel-5 cells to 1.7 μM **2** resulted in a marked and significant reduction (−80 ± 4%, $P <$ 0.01) in the total amount of telomeric 3′-overhang (Fig. 5B), which was paralleled by a significant decrease in the amounts of both the telomere-associated proteins TRF2 (−54.8 ± 4.9%; $P <$

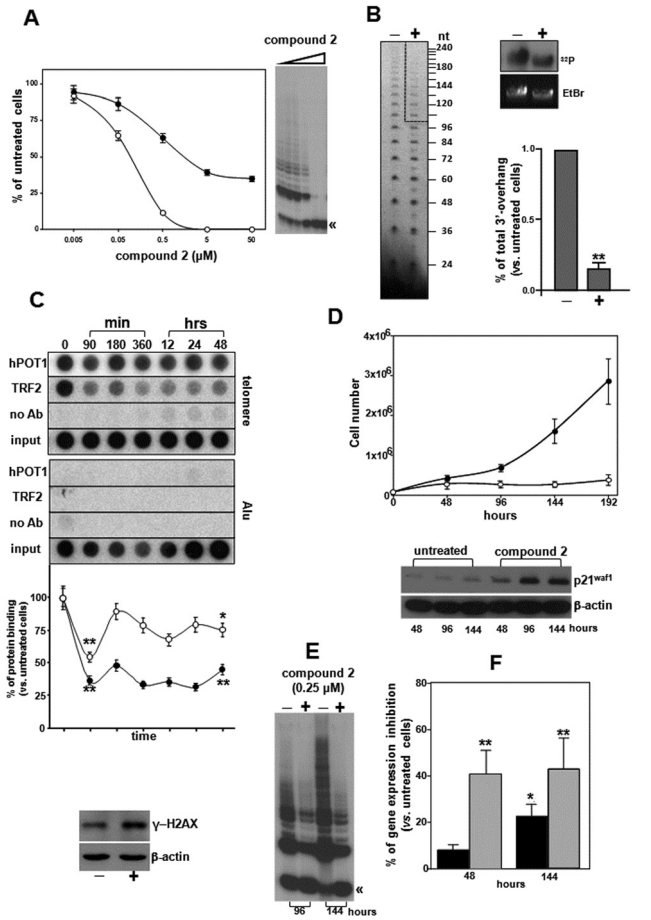

Fig. 5 Biological effects of **2**. (A) Cell growth (●) and telomerase activity (○) inhibition curves after a 48 h exposure of SKMel-5 cells to increasing concentrations of **2**. Data are reported as a percentage of growing cells and telomerase activity compared to untreated cells (mean values ± s.d.). A representative TRAP assay showing the drug-mediated inhibition of telomerase activity has been reported. (B) Representative t-OLA autoradiograph (*left panel*) from untreated or **2**-treated cells. Dashed line shows the reduction of telomeric-3′-overhang length in drug-treated cells. The size (nt) of ligated products is indicated. Representative agarose gels showing the overall amount of 3′-overhangs from in solution hybridization and EtBr staining of total DNA (*right panels*) used as loading control are displayed. Data have been plotted as percentage of total 3′-overhang with respect to untreated cells. (−): no drug; (+): 1.7 μM **2**. (C) Representative time-course ChIP experiments showing the displacement of TRF2 and hPOT1 from telomeres. Data quantification (*lower panel*) shows the dynamic displacement of TRF2 (●) and hPOT1 (○) in **2**-treated cells. Data are reported as percentages with respect to untreated samples. A representative western immunoblot showing the expression levels of γ-H2AX has been also reported. (D) Growth curves of SK-Mel5 cells untreated (●) and after treatment (○) with 0.25 μM **2** (*upper panel*). Data are reported as number of growing cells (mean values ± s.d.). Representative western blotting (*lower panel*) showing the effects of treatment reiteration on the expression levels of $p21^{waf1}$. (E) Representative TRAP assay showing the effect of reiterated treatment on telomerase activity in SKMel5 cells. (F) Quantification of data from qRT-PCR experiments. Data are reported as percentage of inhibition of *c-myc* (black bars) and *hTERT* (gray bars) mRNA expression levels in **2**-treated compared to untreated cells. («): the 36-bp internal TRAP assay standard. β-Actin was used to ensure equal protein loading. *$P < 0.05$; **$P < 0.01$.

0.01) and hPOT1 (−25 ± 1.9%; $P < 0.05$) bound to telomeric sequences (Fig. 5C). Such an effect was already appreciable after a 90 min drug exposure (−64 ± 5.8% and −45.4 ± 3.3%; $P < 0.01$, for TRF2 and hPOT1, respectively) and persisted over the time interval considered, although with a slightly different extent and kinetics (Fig. 5C). These findings indicate that **2** was able to markedly interfere with telomere architecture, leading to dysfunctional/uncapped telomeres.

Consistent with previous findings showing that the G4-ligand Ant1,5 induced a DDR (DNA damage response) in melanoma cells,[30] we observed that the **2**-mediated displacement of TRF2 and hPOT1 from the telomeres was paralleled by a marked increase in γ-H2AX expression levels (Fig. 5C). This evidence is consistent with the observation that short-term exposure of cancer cells to high doses of G4 ligands results in telomere uncapping and accumulation of γ-H2AX.[3,29,31–33] In keeping with the notion that telomerase can be indirectly inhibited by telomeric G4 ligand, due to its inability to extend a G4-folded substrate, we assessed the enzyme's catalytic activity in protein extracts obtained from SKMel-5 cells exposed to the same drug concentrations used for the cytotoxicity evaluation. Such an analysis revealed a marked and dose-dependent decrease in telomerase activity, which was completely inhibited at the highest drug concentrations (Fig. 5A).[34]

It has been reported that long-term exposure of human cancer cells to subtoxic doses of telomeric G4 ligands induced progressive telomere shortening and replicative senescence, as a consequence of telomerase activity inhibition.[35] On the basis of this evidence, we assessed whether **2** induces a delayed effect on cell growth, by prolonging cell treatment up to 8 days. For this purpose, cells were exposed to 0.25 μM **2**, a drug concentration that did not significantly impair the growth of SKMel-5 cells, when evaluated at 48 h, but induced a marked inhibition of telomerase activity (Fig. 5A). The treatment was reiterated every 48 h and cell growth assessed every 2 days. As reported in Fig. 5D, the total number of **2**-treated cells remained essentially constant during the time-course of the experiment, compared to the exponentially growing control cells. In addition, a time-dependent increase in the expression levels of the cyclin-dependent kinase inhibitor $p21^{waf1}$, which contributes to a senescent phenotype triggered by dysfunctional telomeres, was observed in 2-treated SKMel5 cells (Fig. 5D). These findings suggest that **2** may induce cell senescence, as previously observed with Ant1,5.[30] Moreover, TRAP assay, carried out after at 96 h and at the end of prolonged treatment, showed a marked reduction in telomerase activity in SKMel-5 cells exposed to subtoxic doses of **2** (Fig. 5E).

Inhibition of the enzyme's catalytic activity seems to primarily occur as a consequence of drug-mediated decrease of *c-myc* and *hTERT* mRNA expression levels (Fig. 5F). In fact, real-time PCR data showed a down-regulation of *c-myc* (8.3 ± 1.6% and 22.2 ± 4.5%) which was paralleled by a significant reduction (40.5 ± 10% and 42.8 ± 12.8%, $P < 0.05$) of *hTERT* expression levels, as assessed after 48 and 144 h of exposure to **2**, respectively. This evidence excludes possible data misinterpretations related to the use of TRAP assay to evaluate native telomerase activity in cells exposed to G4 ligands.

Consistent with our findings is the notion that G4-forming regions within the *c-myc* promoter play a critical role in regulating the expression of the gene. In this context, it has been demonstrated that the cationic porphyrin TMPyP4 was able to prolong survival and decrease tumor growth rates in xenograft tumor models due to its ability to down-regulate the expression levels of *c-myc*, which in turn resulted in the transcriptional repression of *hTERT*.[36] Similarly, long-term exposure of leukemia cells to the cryptolepyne derivative SYUIQ-5, a telomeric G4 ligand, triggered *c-myc* promoter and telomerase activity inhibition.[37]

It has been recently reported that the *hTERT* promoter contains 12 consecutive G-tracts – embracing three Sp1 binding sites – that may form multiple G4s.[38] The formation of this tandem G4 structure masks all three Sp1 binding sites, and is predicted to inhibit *hTERT* promoter activity. In this context, our data implies that inhibition of telomerase activity by **2** may be a direct consequence of the stabilization of G4s within the *hTERT* and, although to a lesser extent, *c-myc* promoters.

A therapeutic advantage regarding G4 ligands resides in the evidence that they may have multiple G4 targets.[36,38–40] It has been recently reported that an NDI derivative inhibited the growth of gastrointestinal stromal tumor cells as a consequence of its ability to interact with G4 located both at telomeres and in the promoter region of the *c-kit*, an oncogene frequently activated in this tumor type.[39] The ability of our NDI series to interfere with G4-forming sequences within the promoters or transcripts of different genes (*e.g.*, *hTERT*, *c-myc*, *c-kit*, *Bcl-2*) is currently under investigation.

Finally, since it has been demonstrated that G4 ligands can inhibit also the growth of ALT cells, an advantage in the use of these compounds is related to their ability to induce antiproliferative effects independently from the TMM operating in the tumor cell. In fact, several G4 ligands (*e.g.*, the triazine derivative 115405, the pentacyclicacridine RHPS4, the telomestatin derivative HXDV and the bisantrene regioisomer Ant1,5) have been shown to inhibit the growth of SV40-immortalized human skin fibroblasts GM847 as well as the human osteogenic sarcoma cell lines Saos-2 and U2Os, that maintain telomere by the ALT pathway.[2,35]

Conclusion

A great number of G4 ligands have been reported and investigated as chemical tools for unravelling the structure complexity and biological functions of G4s.[41] Our study represents the first step towards the rational design and synthesis of new molecular devices capable of G4 selective recognition and triggerable covalent damage–stabilization of G4 structures. Although further work is required to both increase alkylation efficiency and characterize the alkylation damage of our NDI derivatives, the development of such small molecules represents an original strategy to achieve the selective and covalent modification of target G4s for therapeutic purposes. In addition, future improvement of our NDIs will provide an original strategy to obtain a genome wide mapping of G4 structures, including those forming within RNA molecules, such as those transcribed from telomeres.[42] In this context, an *in silico* analysis has recently identified ~400 000 sequences within the human genome that could form G4 structures,[8] leading to the notion that G4s may play a pivotal

role in key biological processes as well as offering the exciting perspective of novel cancer-related target identification.

Although the therapeutic approaches based on G4 targeting are still in their infancy, accumulating evidence indicates that telomeric G4 stabilizing agents are able to selectively impair the growth of cancer cells without affecting the viability of normal cells.[2,35] This observation, along with the recently completed phase I–II clinical trials with the G4 binder quarfloxin (www.ClinicalTrial.gov), points to G4 ligands as possible drug candidates for future clinical applications.

Experimental

Microwave assisted synthesis of the NDIs

The NDI **9**[14] (250 mg, 0.4 mmol) and the corresponding amine (**11** and **12**,[11] 0.6 mmol) were heated in DMF in a microwave reactor (closed vessel) at 180 °C, 200 psi and 200 W for 3–10 min. The violet solution was cooled at r.t. and water (50 ml) was added to induce precipitation. The filtered crude was purified by HPLC, using a C-18 reverse phase column ($CH_3CN : H_2O$ 0.1% TFA, as eluent). Addition of 0.5 ml HCl 1 M solution to each chromatographic portion and solvent evaporation under vacuum afforded adducts **1**, **1Br**, **2**, **2Br**, and **6** as hydrochlorides.

***N,N′*-Bis-((dimethylamino)ethylamino)-2-(2-(3-(dimethylamino) methyl-4-hydroxy phenyl)ethylamino)-1,4-5,8-naphthalenetetracarboxylic bisimide trihydrochloride**

(**2**·3HCl): Red solid. M.p. dec. >350 °C. ^{1}H NMR(CD_3OD, 300 MHz): δ = 8.36 (d, 1H, J = 7.8 Hz); 8.08 (d, 1H, J = 7.8 Hz); 7.94 (s, 1H); 7.40 (s, 1H); 7.37 (d, 1H, J = 8.4 Hz); 6.96 (d, 1H, J = 8.4 Hz); 4.53–4.52 (m, 4H); 4.34 (s, 2H); 3.82 (t, 2H, J = 6.8 Hz); 3.60–3.54 (m, 4H); 3.05 (s, 14H); 2.90 (s, 6H). ^{13}C NMR (CD_3OD): δ = 167.4; 165.1; 165.0; 164.7; 157.0; 153.7; 134.3; 133.8; 132.3; 131.5; 131.0; 129.0; 127.4; 125.6; 124.5; 121.3; 120.7; 118.3; 117.2; 100.5; 65.2; 57.6; 57.3; 45.9; 44.4; 44.3; 43.6; 37.2; 36.8; 35.7. Elemental analysis (%) calcd for $C_{33}H_{43}Cl_3N_6O_5$: C, 55.82; H, 6.10; Cl, 14.98; N, 11.84; O, 11.27. Found C, 55.78; H, 6.19; Cl, 15.03; N, 11.82.

***N,N′*-Bis-((dimethylamino)ethylamino)-2-bromo-6-(2-(3-(dimethylamino)methyl-4-hydroxyphenyl)ethylamino)-1,4-5,8-naphthalenetetracarboxylic bisimide trihydrochloride**

(**2Br**·3HCl): Blue solid. M.p. dec. >350 °C. ^{1}H NMR (CD_3OD, 300 MHz): δ = 8.44 (s, 1H); 8.15 (s. 1H); 7.15 (d, 1H, J = 8.2 Hz); 6.91 (s, 1H); 6.80 (d, 1H, J = 8.2 Hz); 4.40–4.33 (m, 4H); 3.73 (m, 2H); 3.65 (s, 2H); 2.99 (m, 2H); 2.71 (bs, 4 H); 2.45 (s, 6H); 2.42 (s, 6H); 2.33 (s, 6H). ^{13}C NMR (CD_3OD): δ = 166.0; 163.2; 161.7; 156.7; 150.9; 149.5; 129.0; 128.6.; 128.4; 126.7; 124.0; 123.4; 122.8; 122.0; 118.4; 116.1; 108.3; 101.1; 62.7; 56.9; 56.8; 45.5; 45.0; 44.4; 44.0; 38.2; 37.7; 35.0; 30.8. Elemental analysis (%) calcd for $C_{33}H_{42}BrCl_3N_6O_5$: C, 50.24; H, 5.37; Br, 10.13; Cl, 13.48; N, 10.65; O, 10.14. Found C, 50.30; H, 5.39; Br, 10.08; Cl, 13.53; N, 10.61.

***N,N′*-Bis-((dimethylamino)ethylamino)-2,6-bis(2-(3-(dimethylamino)methyl-4-hydroxyphenyl)ethylamino)-1,4-5,8-naphthalenetetracarboxylic bisimide tetrahydrochloride (6·4HCl).** Violet solid. M.p. dec. >350 °C. ^{1}H NMR (CD_3OD, 300 MHz): δ = 8.50 (s, 2H); 7.17 (m, 4H); 6.82 (d, 2H, J = 10.3 Hz); 4.57 (m, 4H); 4.26 (s, 4H); 3.60 (t, 4H, J = 7.7 Hz); 3.31 (m, 4H); 3.04 (s, 12H); 2.84 (s, 12H); 2.72 (s, 4H). ^{13}C NMR (CD_3OD): δ = 173.5; 165.4; 156.5; 152.5; 133.8; 133.6; 132.4; 126.4; 125.5; 125.0; 117.8; 116.7; 108.4; 58.7; 57.8; 44.8; 44.4; 43.5; 42.3; 37.4; 35.8; 28.3; 22.8. Elemental analysis (%) calcd for $C_{44}H_{60}C_{l4}N_8O_6$: C, 56.29; H, 6.44; Cl, 15.11; N, 11.94; O, 10.23. Found C, 56.32; H, 6.41; Cl, 15.18; N, 12.00.

Nucleophilic aromatic substitution reaction at r.t.

The NDI **9** (250 mg, 0.4 mmol) was dissolved into 20 ml of DMF in a round bottom flask together with the corresponding amine (**11**, **13** and **14**; 0.6 mmol). The mixture was stirred at r.t. for 8–48 h under argon. The resulting red solution was poured in water (100 ml) and filtered. The solid collected was washed with water and purified by preparative HPLC chromatography ($CH_3CN : H_2O$, 0.1% TFA). HCl 1 M solution was added to each chromatographic portion. Solvent evaporation under vacuum afforded the adducts **1**, **1Br**, **3**, **3Br** and **4** as hydrochlorides.

Acknowledgements

This work was supported by MIUR, Grant FIRB-Ideas RBID082ATK, Grants AIRC 5826 and 8861 (Associazione Italiana per la Ricerca sul Cancro) and by Pavia University. The use of FLAP software is a courtesy of Molecular Discovery Ltd, UK. We thank Dr Giovanna Sattin and Dr Daniele Dal Zoppo (University of Padova) for assistance with the MS experiments.

Notes and references

1 D. Hanahan and R. A. Weinberg, *Cell*, 2011, **5**, 646.
2 M. Folini, L. Venturini, G. Cimino-Reale and N. Zaffaroni, *Expert Opin. Ther. Targets*, 2011, **15**, 579.
3 T. De Lange, *Science*, 2009, **5955**, 948.
4 J.-D. Henson and R.-R. Reddell, *FEBS Lett.*, 2010, **584**, 3800.
5 A.-J. Cesare and R.-R. Reddell, *Nat. Rev. Genet.*, 2010, **11**, 19.
6 J.-W. Shay and W.-E. Wright, *Nat. Rev. Drug Discovery*, 2006, **5**, 577.
7 A. Roth, C.-B. Heraly and G.-M. Baerlocher, *Recent Results Cancer Res.*, 2010, **184**, 221.
8 T.-M. Bryan and P. Baumann, *Methods Mol. Biol.*, 2010, **608**, 1.
9 D. Monchaud and M.-P. Teulade-Fichou, *Org. Biomol. Chem.*, 2008, **6**, 627.
10 H. Bertrand, S. Bombard, D. Monchaud, E. Talbot, A. Guedin, J.-L. Mergny, R. Grunert, P.-J. Bednarskid and M.-P. Teulade-Fichou, *Org. Biomol. Chem.*, 2009, **6**, 2866.
11 M. Di Antonio, F. Doria, S.-N. Richter, C. Bertipaglia, M. Mella, C. Sissi, M. Palumbo and M. Freccero, *J. Am. Chem. Soc.*, 2009, **131**, 13132.
12 F. Cuenca, O. Greciano, M. Gunaratnam, S. Haider, D. Munnur, R. Nanjunda, W.-D. Wilson and S. Neidle, *Bioorg. Med. Chem. Lett.*, 2008, **18**, 1668.
13 S.-M. Hampel, A. Sidibe, M. Gunaratnam, J.-F. Riou and S. Neidle, *Bioorg. Med. Chem. Lett.*, 2010, **20**, 6459.
14 M. Nadai, F. Doria, M. Di Antonio, G. Sattin, L. Germani, C. Percivalle, M. Palumbo, R. S. Richter and M. Freccero, *Biochimie*, 2011, **93**, 1328.
15 S. Cross, M. Baroni, E. Casorati, P. Benedetti and S. Clementi, *J. Chem. Inf. Model.*, 2010, **50**, 1442.

16 S. Cross and G. Cruciani, *Drug Discovery Today*, 2010, **15**, 23.
17 S. Alcaro, A. Artese, G. Costa, S. Distinto, F. Ortuso and L. Parrotta, *Biochimie*, 2011, **93**, 1267.
18 K.-N. Luu, A.-T. Phan, V. V. Kuryavyi, L. Lacroix and D.-J. Patel, *J. Am. Chem. Soc.*, 2006, **128**, 9963.
19 A. Ambrus, D. Chen, J. Dai, T. Bialis, R.-A. Jones and D. Yang, *Nucleic Acids Res.*, 2006, **34**, 2723.
20 M. Vorlickova, J. Chladkova, I. Kejnovska, M. Fialova and J. Kypr, *Nucleic Acids Res.*, 2005, **33**, 5851.
21 Y. Xue, J.-Q. Liu, K.-W. Zheng, Z.-Y. Kan, Y.-H. Hao and Z. Tan, *Angew. Chem., Int. Ed.*, 2011, **50**, 8046.
22 S. Goutelle, M. Maurin, F. Rougier, X. Barbaut, L. Bourguignon, M. Ducher and P. Maire, *Fundam. Clin. Pharmacol.*, 2008, **22**, 633.
23 G.N. Parkinson, F. Cuenca and S. Neidle, *J. Mol. Biol.*, 2008, **381**, 1145.
24 J.-H. Tan, T.-M. Ou, J.-Q. Hou, Y.-J. Lu, S.-L. Huang, H.-B. Luo, J.-Y. Wu, Z.-S. Huang, K.-J. Wong and L.-Q. Gu, *J. Med. Chem.*, 2009, **52**, 2825.
25 M. Freccero, C. Valentin and M. Sarzi-Amade, *J. Am. Chem. Soc.*, 2003, **125**, 3544.
26 W.-F. Veldhuyzen, Y.-F. Lam and S.-E. Rokita, *Chem. Res. Toxicol.*, 2001, **14**, 1345.
27 S.-E. Rokita, J. Yang, P. Pande and W.-A. Greenberg, *J. Org. Chem.*, 1997, **62**, 3010.
28 M. Freccero, R. Gandolfi and M. Sarzi-Amade, *J. Org. Chem.*, 2003, **68**, 6411.
29 F. Cuenca, M.-J. Moore, K. Johnson, B. Guyen, A. De Cian and S. Neidle, *Bioorg. Med. Chem. Lett.*, 2009, **19**, 5109.
30 M. Folini, C. Pivetta, G. Zagotto, C. De Marco, M. Palumbo, N. Zaffaroni and C. Sissi, *Biochem. Pharmacol.*, 2010, **12**, 1781.
31 E. Salvati, C. Leonetti, A. Rizzo, M. Scarsella, M. Mottolese, R. Galati, L. Sperduti, M.-F. Stevens, M. D'Incalci and M. Blasco, *et al.*, *J. Clin. Invest.*, 2007, **117**, 3236.
32 A. Rizzo, E. Salvati, M. Porru, C. D'Angelo, M. F. Stevens, M. D'Incalci, C. Leonetti, E. Gilson, G. Zupi and A. Biroccio, *Nucleic Acids Res.*, 2009, **37**, 5353.
33 Y.-C. Tsai, H. Qi, C.-P. Lin, R.-K. Lin, J.-E. Kerrigan, S.-G. Rzuczek, E.-J. LaVoie, J.-E. Rice, D.-S. Pilch and Y.-L. Lyu, *et al.*, *J. Biol. Chem.*, 2009, **284**, 22535.
34 To ensure that all the excess of drug was removed before performing the TRAP assay, the SKMel-5 cells exposed to the different drug concentrations were first harvested and washed 3 times with phosphate buffered saline. Subsequently protein extraction was performed.
35 M. Folini, P. Gandelini and N. Zaffaroni, *Biochim. Biophys. Acta*, 2009, **1792**, 309.
36 C.-L. Grand, H. Han, R.-M. Muñoz, S. Weitman, D.-D. Von Hoff, L.-H. Hurley and D.-J. Bearss, *Mol. Cancer Ther.*, 2002, **1**, 565.
37 J.-N. Liu, R. Deng, J.-F. Guo, J.-M. Zhou, G.-K. Feng, Z.-S. Huang, L.-Q. Gu, Y.-X. Zeng and X.-F. Zhu, *Leukemia*, 2007, **21**, 1300.
38 S.-L. Palumbo, S. W. Ebbinghaus and L.-H. Hurley, *J. Am. Chem. Soc.*, 2009, **131**, 10878.
39 D. Gomez, T. Lemarteleur, L. Lacroix, P. Mailliet, J.-L. Mergny and J.-F. Riou, *Nucleic Acids Res.*, 2004, **32**, 371.
40 M. Gunaratnam, S. Swank, S.-M. Haider, K. Galesa, A.-P. Reszka, M. Beltran, F. Cuenca, J.-A. Fletcher and S. Neidle, *J. Med. Chem.*, 2009, **52**, 3774.
41 N.-W. Luedtke, *Chimia*, 2009, **63**, 134.
42 G.-W. Collie, S. Sparapani, G.-N. Parkinson and S. Neidle, *J. Am. Chem. Soc.*, 2011, **133**, 2721.

